PNAS RESEARCH ARTICLE | IMMUNOLOGY AND INFLAMMATION

Mitochondrial calcium uniporter promotes phagocytosis-dependent activation of the NLRP3 inflammasome

Hong Dong[a], Bao Zhao[a], Jianwen Chen[a], Zihao Liu[a], Xinghui Li[a], Lupeng Li[b], and Haitao Wen[a,c,d,1]

Edited by Katherine Fitzgerald, University of Massachusetts Medical School, Worcester, MA; received December 23, 2021; accepted May 9, 2022

Mitochondria, a highly metabolically active organelle, have been shown to play an essential role in regulating innate immune function. Mitochondrial Ca^{2+} uptake via the mitochondrial Ca^{2+} uniporter (MCU) is an essential process regulating mitochondrial metabolism by targeting key enzymes involved in the tricarboxylic acid cycle (TCA). Accumulative evidence suggests MCU-dependent mitochondrial Ca^{2+} signaling may bridge the metabolic reprogramming and regulation of immune cell function. However, the mechanism by which MCU regulates inflammation and its related disease remains elusive. Here we report a critical role of MCU in promoting phagocytosis-dependent activation of NLRP3 (nucleotide-binding domain, leucine-rich repeat containing family, pyrin domain-containing 3) inflammasome by inhibiting phagolysosomal membrane repair. Myeloid deletion of MCU ($Mcu^{\Delta mye}$) resulted in an attenuated phagolysosomal rupture, leading to decreased caspase-1 cleavage and interleukin (IL)-1β release, in response to silica or alum challenge. In contrast, other inflammasome agonists such as adenosine triphosphate (ATP), nigericin, poly(dA:dT), and flagellin induced normal IL-1β release in $Mcu^{\Delta mye}$ macrophages. Mechanistically, we demonstrated that decreased NLRP3 inflammasome activation in $Mcu^{\Delta mye}$ macrophages was caused by improved phagolysosomal membrane repair mediated by ESCRT (endosomal sorting complex required for transport)-III complex. Furthermore, $Mcu^{\Delta mye}$ mice showed a pronounced decrease in immune cell recruitment and IL-1β production in alum-induced peritonitis, a typical IL-1–dependent inflammation model. In sum, our results identify a function of MCU in promoting phagocytosis-dependent NLRP3 inflammatory response via an ESCRT-mediated phagolysosomal membrane repair mechanism.

inflammasome | phagosome | MCU | ESCRT

Significance

Mitochondrial Ca^{2+} uniporter (MCU) has been recently reported to be involved in activation of the NLRP3 inflammasome due to mitochondrial damage. However, whether MCU is a general regulator of NLRP3 inflammasome and the overall effect of MCU on inflammation remain elusive. Here, we show that deletion of MCU causes no general defect in NLRP3 inflammasome activation. Instead, MCU is uniquely required for phagocytosis-triggered activation of NLRP3 inflammasome by counteracting ERCRT complex–mediated phagolysosomal membrane repair. Our data also suggest a proinflammatory effect of myeloid-derived MCU in an alum-induced peritonitis model. Therefore, our study provides genetic evidence to clarify the innate immune function of MCU.

The NLRP3 (nucleotide-binding domain, leucine-rich repeat–containing family, pyrin domain–containing 3) inflammasome is a multiprotein cytosolic complex consisting of the NLRP3, the adaptor ASC, and the effector molecule caspase-1 (1, 2). Activation of the NLRP3 inflammasome leads to the induction of caspase-1 activity, which subsequently mediates the maturation and secretion of inflammatory cytokines IL-1β and IL-18, as well as gasdermin-dependent pyroptosis (3, 4). A diverse series of exogenous and endogenous agonists can activate the NLRP3 inflammasome via either phagosome-dependent or -independent pathways (5, 6). It is generally realized that the activating effects of various NLRP3 stimuli converge on the loss of cellular ion homeostasis, leading to the assembly of multiprotein complex and activation of the NLRP3 inflammasome. For example, numerous studies have revealed potassium efflux as an essential step for activation of the NLRP3 inflammasome in response to various stimuli (6, 7). In addition, several studies reported that cytosolic influx of Ca^{2+} from either extracellular space (8–10) or endoplasmic reticulum (ER) (11) was required for NLRP3 inflammasome activation.

Mitochondrial Ca^{2+} signaling is a fundamental mechanism regulating mitochondrial metabolism by targeting key enzymes involved in the tricarboxylic acid (TCA) cycle (12). Mitochondrial Ca^{2+} uniporter (MCU) is a highly selective calcium channel, which is required for mitochondrial uptake of cytosolic Ca^{2+} after the influx of extracellular Ca^{2+} or the release of the ER Ca^{2+} pool (13–16). In addition to regulating intramitochondrial metabolic processes, MCU also contributes to buffering cytosolic Ca^{2+} peaks (17), thus potentially affecting extramitochondrial signaling cascades. This is particularly relevant to immune cell functions due to an essential role of Ca^{2+} signaling regulating numerous immune signaling pathways through a variety of molecular mechanisms. Our recent study using *Mcu* gene-deletion ($Mcu^{\Delta mye}$) macrophages demonstrated that MCU-mediated acetyl-CoA metabolism modulated bactericidal response by targeting LC3-associated phagocytosis (LAP), an uncanonical autophagic process characterized by LC3-decorated single-membrane vacuoles (18). Other studies revealed

Author affiliations: [a]Department of Microbial Infection and Immunity, The Ohio State University, Columbus, OH 43210; [b]Department of Microbiology and Immunology, University of North Carolina at Chapel Hill, Chapel Hill, NC 27599; [c]The Ohio State University Comprehensive Cancer Center, The Ohio State University, Columbus, OH 43210; and [d]Pelotonia Institute for Immuno-Oncology, The Ohio State University Comprehensive Cancer Center, The Ohio State University, Columbus, OH 43210

Author contributions: H.D. and H.W. designed research; H.D., B.Z., J.C., Z.L., X.L., and L.L. performed research; H.D. and H.W. analyzed data; and H.D. and H.W. wrote the paper.

The authors declare no competing interest.

This article is a PNAS Direct Submission.

[1]To whom correspondence may be addressed. Email: Haitao.Wen@osumc.edu.

This article contains supporting information online at http://www.pnas.org/lookup/suppl/doi:10.1073/pnas.2123247119/-/DCSupplemental.

Published June 22, 2022.

MCU as a positive regulator of the NLRP3 inflammasome in response to the challenge with bacteria (19, 20) or complement membrane attack complex (21). However, whether MCU is a general regulator of the NLRP3 inflammasome and the underlying mechanism remains unclear.

Recent studies have identified the endosomal sorting complex required for transport (ESCRT) protein complex essential for phagolysosomal membrane repair when damaged by various stimuli (22, 23). The first step of ESCRT-mediated membrane repair is cytosolic Ca^{2+}-trigged recruitment of ESCRT proteins to the damaged membrane site, which depends on the Ca^{2+} binding protein, apoptosis-linked gene (ALG)-2 and ALG-2–interacting protein X (ALIX, also known as programmed cell death 6 interacting protein, PDCD6IP) (24, 25). The second step is the pinching out of damaged membrane controlled by ESCRT complex subunits such as charged multivesicular body protein 4B (CHMP4B) and others (22, 24, 26, 27). The importance of ESCRT-mediated membrane repair in prevention of inflammation has been reported (27, 28).

In this study, we report that MCU is not a general regulator of the NLRP3 inflammasome, or the NLRC4 or absent in melanoma (AIM2) inflammasome. Instead, MCU is uniquely required for maximal activation of the NLRP3 inflammasome via a phagocytosis route by inhibiting phagolysosomal membrane repair. Mechanistically, MCU-mediated mitochondrial Ca^{2+} uptake attenuates ESCRT-mediated phagolysosomal membrane repair by buffering the cytosolic Ca^{2+} peak. Deletion of MCU in myeloid cells resulted in an attenuated inflammatory response in an alum-induced peritonitis model, therefore highlighting the therapeutic potential of MCU in the treatment of inflammatory diseases (20).

Results

MCU Specifically Promotes Phagocytosis-Triggered NLRP3 Inflammasome Activation. Previous studies suggest that inhibition of MCU results in decreased production of IL-1β and IL-18 in human epithelial cells derived from patients with cystic fibrosis in response to bacterial challenge (19, 20). It has been well established that the processing and production of IL-1β and IL-18 requires first, a priming step with a number of stimuli, including the Toll-like receptor 4 (TLR4) agonist lipopolysaccharide (LPS), and second, a signal to activate the inflammasome (1, 2). To determine which of the NLRP3, NLRC4, and AIM2 inflammasomes is affected by MCU, we challenged LPS-primed bone marrow-derived macrophages (BMMs) generated from $Mcu^{\Delta mye}$ mice or wild-type (WT) control $Mcu^{fl/fl}$ mice (18) with stimulating agonists for individual inflammasomes. Dosage-dependent production of IL-1β and cytotoxicity, as assayed by lactate dehydrogenase (LDH) release, were detected in $Mcu^{fl/fl}$ BMMs when challenged with silica (Fig. 1*A* and *SI Appendix*, Fig. S1 *A* and *C*) or alum (Fig. 1*B* and *SI Appendix*, Fig. S1 *B* and *D*), two widely used NLRP3 inflammasome agonists through the phagocytosis route. However, significantly less IL-1β production and cytotoxicity were observed in similarly treated $Mcu^{\Delta mye}$ BMMs, indicating an impaired NLRP3 inflammasome activation. Surprisingly, stimulation with adenosine triphosphate (ATP) (Fig. 1*C*) or nigericin (Fig. 1*D*), two phagocytosis-independent agonists for the NLRP3 inflammasome, revealed normal IL-1β production and cytotoxicity in $Mcu^{\Delta mye}$ BMMs, suggesting that MCU is not a general mediator of the NLRP3 inflammasome. Production of inflammasome-independent cytokine IL-6 was normal in $Mcu^{\Delta mye}$ BMMs, indicating an intact priming of the NLRP3 inflammasome by LPS (Fig. 1*E* and *SI Appendix*, Fig. S1 *E* and *F*). Moreover, $Mcu^{\Delta mye}$ BMMs produced comparable amounts of transcripts of cytokine genes (*Il1a*, *Il1b*, *Il6*, *Il12a*, *Il12b*, *Tnfa*, *Cxcl1*, *Cxcl2*, and *Il10*) (*SI Appendix*, Fig. S1*G*) and IL-6 and TNF-α protein (*SI Appendix*, Fig. S1*H*) in response to LPS or another two TLR agonists Pam3Cys (TLR2) and CpG (TLR9) (*SI Appendix*, Fig. S1*I*) compared to $Mcu^{fl/fl}$ BMMs. Moreover, activation of innate immune signaling such as the NF-κB and MAPK pathways was similarly induced by LPS between MCU-sufficient and -deficient BMMs (*SI Appendix*, Fig. S1*J*). In sum, deletion of MCU causes impaired activation of the NLRP3 inflammasome specifically in response to phagocytosis-dependent stimuli.

We further examined whether MCU is important for activation of the AIM2 and NLRC4 inflammasome. Poly(dA:dT) and flagellin are commonly used agonists that activate the AIM2 and NLRC4 inflammasome, respectively (1, 2). $Mcu^{\Delta mye}$ BMMs produced comparable amounts of IL-1β and IL-6 when transfected with poly(dA:dT) (Fig. 1*F*) and flagellin (Fig. 1*G*) compared with similarly treated $Mcu^{fl/fl}$ cells. Therefore, MCU is dispensable for AIM2 and NLRC4 inflammasome activation. We next evaluated inflammasome activation by examining the cleavage of procaspase-1 and pro–IL-1β and the formation of ASC specks, two hallmarks of inflammasome activation. Stimulation with silica induced the cleavage of procaspase-1 and pro–IL-1β in LPS-primed $Mcu^{fl/fl}$ BMMs. However, these effects were severely attenuated in $Mcu^{\Delta mye}$ BMMs (Fig. 1*H*). Meanwhile, $Mcu^{\Delta mye}$ BMMs exhibited normal cleavage of procaspase-1 and pro–IL-1β when stimulated with ATP (Fig. 1*I*), nigericin (Fig. 1*J*), poly(dA:dT) (Fig. 1*K*), or flagellin (Fig. 1*L*). Immunostaining for ASC revealed a significantly lower percentage of $Mcu^{\Delta mye}$ BMMs containing ASC specks following the challenge with silica for 4 or 8 h compared with $Mcu^{fl/fl}$ BMMs (Fig. 1*M* and *SI Appendix*, Fig. S1*K*). In contrast, stimulation with nigericin, poly(dA:dT), or flagellin induced ASC speck formation at similar levels between $Mcu^{fl/fl}$ and $Mcu^{\Delta mye}$ BMMs (Fig. 1*M*). Collectively, these results indicate that MCU is uniquely required for phagocytosis-triggered activation of the NLRP3 inflammasome, but not required for phagocytosis-independent NLRP3 inflammasome activation or activation of the AIM2 and NLRC4 inflammasome.

Improved Phagolysosome Integrity in $Mcu^{\Delta mye}$ Macrophages after Silica Stimulation. We next sought to determine the mechanism by which MCU promotes phagocytosis-triggered NLRP3 inflammasome activation. Our recent study suggests enhanced assembly and function of LAP in $Mcu^{\Delta mye}$ macrophages, which contributes to an improved bactericidal effect. We therefore employed a genetic strategy to examine whether the impaired NLRP3 inflammasome activation in response to silica challenge involved altered LAP function in $Mcu^{\Delta mye}$ macrophages. However, deletion of neither Rubicon (encoded by the *Rubcn* gene) (*SI Appendix*, Fig. S2*A*) nor NOX2 (encoded by the *Cybb* gene) (*SI Appendix*, Fig. S2*B*), two critical molecules for LAP assembly, was able to rescue impaired IL-1β production in LPS-primed $Mcu^{\Delta mye}$ macrophages following silica challenge. These results clearly indicated that LAP was not responsible for attenuated phagocytosis-dependent activation of the NLRP3 inflammasome in $Mcu^{\Delta mye}$ macrophages. Since LAP formation requires the engagement of TLR signaling inside phagosomes (29), we reasoned that phagocytosis of silica might not induce the assembly of LAP in macrophages primed with extracellular LPS. Indeed, LPS-primed BMMs generated from GFP-LC3 transgenic mice failed to exhibit LC3 puncta

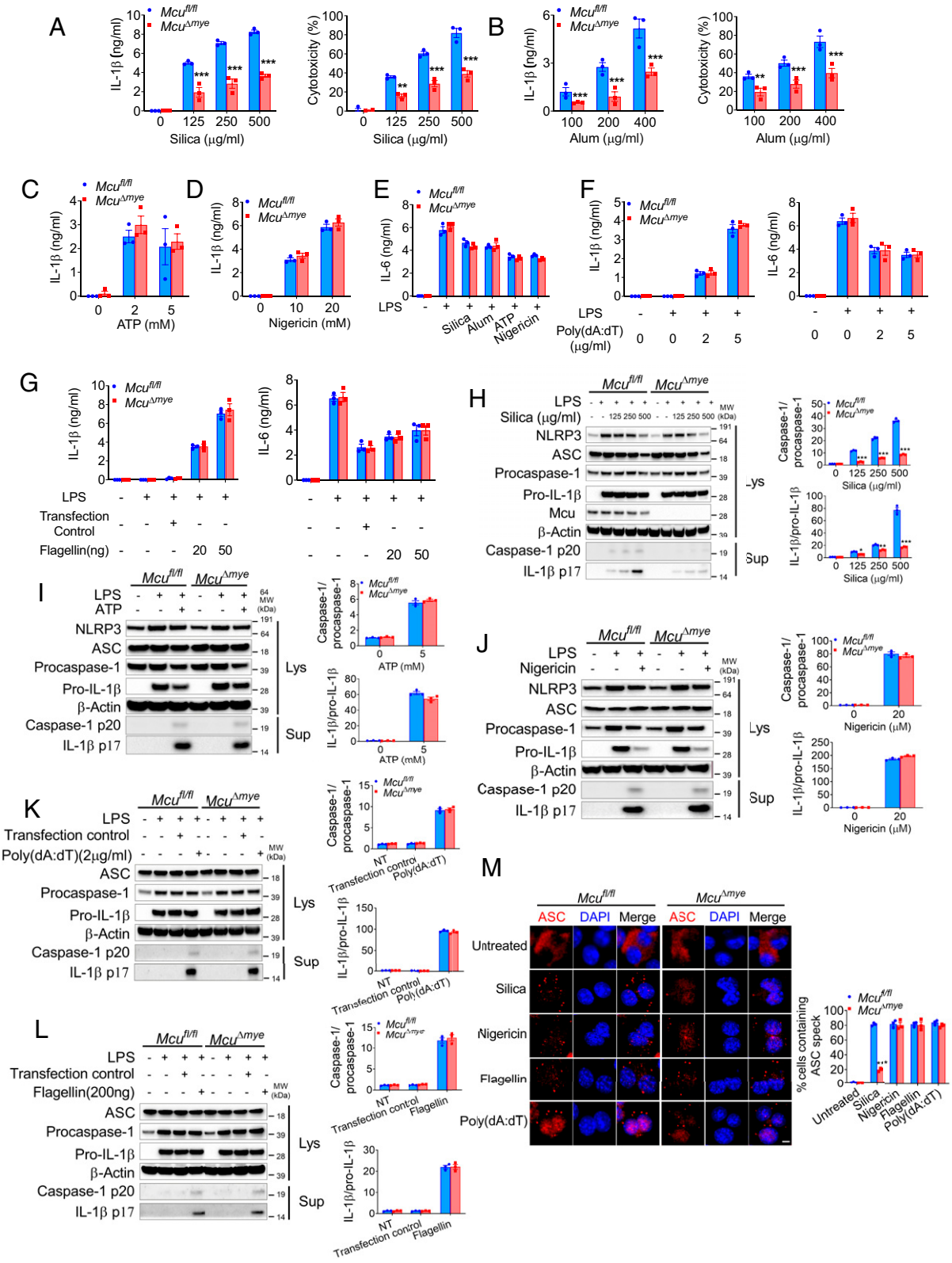

Fig. 1. MCU is uniquely required for phagocytosis-triggered activation of the NLRP3 inflammasome. (*A–G*) *Mcu*$^{fl/fl}$ or *Mcu*$^{\Delta mye}$ BMMs were primed with LPS (200 ng/mL) for 3 h, followed by the stimulation of the NLRP3 inflammasome: silica (*A, E*) and alum (*B, E*) for 4 h and ATP (*C, E*) and nigericin (*D, E*) for 40 min; AIM2 inflammasome: transfected poly (dA:dT) (*F*) for 4 h, or NLRC4 inflammasome: transfected flagellin (*G*) for 4 h. IL-1β and IL-6 in supernatants were measured by ELISA. Cell death was measured by LDH release assay. (*H–L*) Resting or LPS-primed *Mcu*$^{fl/fl}$ or *Mcu*$^{\Delta mye}$ BMMs were stimulated with a series of agonists at indicated dosages, including silica (*H*), ATP (*I*), nigericin (*J*), transfected poly (dA:dT) (*K*), and transfected flagellin (*L*). Immunoblotting was performed to measure the protein levels of indicated molecules in cell lysates (Lys) and supernatants (Sup). Quantitation (*Right*) of expression of active protein versus inactive forms for caspase-1 and IL-1β. (*M*) Microscopy analysis (*Left*) and quantitation (*Right*) of ASC speck formation in LPS-primed *Mcu*$^{fl/fl}$ or *Mcu*$^{\Delta mye}$ BMMs stimulated with indicated agonists. Values are expressed as mean ± SEM, and the results are representative of three independent experiments. (Scale bar, 2 μm.) Statistical analysis was determined by *t* test; **P* < 0.05, ***P* < 0.01, ****P* < 0.001.

following silica challenge, indicating no efficient LAP formation. As a positive control, phagocytosis of zymosan, a particle structure containing agonists for TLR2 and dectin-1, induced strong LAP formation (*SI Appendix*, Fig. S2*C*) (29). Therefore, MCU promotes phagocytosis-triggered NLRP3 inflammasome activation via a LAP-independent manner, presumably due to the lack of LAP induction during silica challenge.

It has been well documented that phagolysosomal rupture following phagocytosis of undegradable crystalline materials leads to activation of the NLRP3 inflammasome (5). We therefore examined phagolysosome integrity in silica-challenged $Mcu^{\Delta mye}$ macrophages. DQ-ovalbumin (OVA) is a phagolysosome-localized fluorescent dye with a localized small vesicle pattern in untreated macrophages (5). As expected, challenge with silica induced the conversion of DQ-OVA fluorescence from a small vesicle pattern to a spread cytosolic pattern in $Mcu^{fl/fl}$ BMMs, indicating the leak of phagolysosomes (Fig. 2*A*). However, a significantly higher number of $Mcu^{\Delta mye}$ macrophages still maintained a small vesicle pattern of DQ-OVA fluorescence, suggesting an improved phagolysosome integrity. We further quantified the degree of phagolysosomal rupture by staining cells with acridine orange, a fluorescent dye that stains acidic lysosomes (5). The amount of red fluorescence of acridine orange directly correlates with the amount of intact acidic lysosomes in macrophages. We found that $Mcu^{\Delta mye}$ macrophages were significantly protected from silica-induced loss of acridine orange staining as assayed by both flow cytometry analysis (Fig. 2*B*) and confocal microscopic assay (Fig. 2*C*). Therefore, these results suggest an improved phagolysosome integrity in $Mcu^{\Delta mye}$ macrophages upon silica challenge.

It has been known that in addition to regulating intramitochondrial signaling, MCU also contributes to buffering cytosolic Ca^{2+} peaks (17). While mitochondrial Ca^{2+} uptake following silica exposure was completely abolished in the absence of MCU (Fig. 2*D*), as expected, we detected a slightly increased cytosolic Ca^{2+} concentration ($[Ca^{2+}]_{cyt}$) in $Mcu^{\Delta mye}$ BMMs compared with $Mcu^{fl/fl}$ BMMs (Fig. 2*E*). It is worth noting that this slight increase in $[Ca^{2+}]_{cyt}$ in $Mcu^{\Delta mye}$ BMMs was unlikely evenly distributed across the cytosolic compartment, since Ca^{2+} peaks much higher in the area close to the mitochondria compared to that in the rest of the cytosol, namely Ca^{2+} hot spots (17). To determine whether increased $[Ca^{2+}]_{cyt}$ contributes to improved phagolysosome integrity in silica-challenged $Mcu^{\Delta mye}$ BMMs, we treated macrophages with the cell-permeable Ca^{2+} chelator Glycine, N,N'-[1,2-ethanediylbis(oxy-2,1-phenylene)]-bis[N-[2-[(acetyloxy)methoxy]-2-oxoethyl]]-, bis[(acetyloxy)methyl] ester (BAPTA-AM) (8, 27, 30). BAPTA-AM treatment completely abolished the increased number of $Mcu^{\Delta mye}$ BMMs with the small vesicle pattern of DQ-OVA fluorescence (Fig. 2*F*) and reversed the decreased number of $Mcu^{\Delta mye}$ BMMs losing acridine orange staining upon silica challenge (Fig. 2*G*). These results indicate that loss of MCU buffering of cytosolic Ca^{2+} peaks results in a less severe phagolysosomal leak via an elevated $[Ca^{2+}]_{cyt}$. Moreover, we found that BAPTA-AM treatment markedly eliminated IL-1β production in both $Mcu^{\Delta mye}$ and $Mcu^{fl/fl}$ BMMs following silica exposure (Fig. 2*H*). This was consistent with a previous study showing an essential role of cytosolic Ca^{2+} directly controlling activation of the NLRP3 inflammasome (8). In sum, the findings reveal an impaired phagocytosis-triggered activation of the NLRP3 inflammasome in the absence of MCU, which correlates with improved phagolysosome integrity.

The ESCRT Complex Attenuates Phagocytosis-Triggered NLRP3 Inflammasome Activation in $Mcu^{\Delta mye}$ Macrophages. Recent studies have identified the ESCRT complex as an essential mediator of phagolysosomal membrane repair (22, 23). ESCRT proteins such as ALIX and CHMP4B localize to the damaged phagolysosome during membrane repair to form a punctate pattern (23). Importantly, the ESCRT-mediated membrane repair mechanism requires an elevated $[Ca^{2+}]_{cyt}$ (27, 31, 32). Since we detected improved phagolysosomal integrity, which correlated with elevated $[Ca^{2+}]_{cyt}$ in silica-exposed $Mcu^{\Delta mye}$ BMMs, we hypothesized that ESCRT-mediated phagolysosomal membrane repair was responsible for impaired NLRP3 inflammasome activation. To this end, we first investigated silica-induced phagolysosomal recruitment of ESCRT components ALIX and CHMP4B. The immunostaining assay revealed increased colocalization of ALIX puncta (Fig. 3*A*) or CHMP4B puncta (Fig. 3*B*) with lysosomal-associated membrane protein 1 (LAMP1), a late phagosomal and lysosomal marker, in silica-challenged $Mcu^{\Delta mye}$ BMMs compared to similarly treated $Mcu^{fl/fl}$ BMMs. Therefore, deletion of MCU leads to enhanced phagolysosomal recruitment of ESCRT proteins upon silica challenge.

We next sought to determine whether deletion of ESCRT components can restore phagolysosomal rupture and NLRP3 inflammasome activation in silica-challenged $Mcu^{\Delta mye}$ BMMs. Immortalized BMMs (imBMMs) (5) generated from $Mcu^{\Delta mye}$ mice exhibited a similar phenotype of impaired silica-triggered NLRP3 inflammasome activation, as evidenced by significantly less IL-1β production and cytotoxicity (*SI Appendix*, Fig. S3*A*) and attenuated cleavage of procaspase-1 and pro–IL-1β (*SI Appendix*, Fig. S3*B*), compared to $Mcu^{fl/fl}$ imBMMs. Stimulation with ATP or nigericin (*SI Appendix*, Fig. S3*C*) induced normal IL-1β production in $Mcu^{\Delta mye}$ imBMMs, as similarly observed in primary BMMs. IL-6 production was also comparable between $Mcu^{fl/fl}$ and $Mcu^{\Delta mye}$ imBMMs (*SI Appendix*, Fig. S3*D*). We further reconstituted $Mcu^{\Delta mye}$ imBMMs with GFP-tagged MCU through a lentivector-based strategy (33) and examined silica-induced NLRP3 inflammasome activation (*SI Appendix*, Fig. S3*E*). Reconstitution with MCU-GFP reversed IL-1β production and cytotoxicity in $Mcu^{\Delta mye}$ imBMMs without affecting IL-6 production, while reconstituting with empty vector did not (*SI Appendix*, Fig. S3 *F* and *G*). Therefore, defective NLRP3 activation in response to phagosome rupture in $Mcu^{\Delta mye}$ macrophages is indeed due to the loss of MCU. Previous studies have demonstrated that CHMP4B and CHMP3 are two essential components of ESCRT-III complex that are required for ESCRT-mediated membrane repair (24, 26, 27). We therefore deleted either the *Chmp4b* gene ($Chmp4b^{-/-}$) or *Chmp3* gene ($Chmp3^{-/-}$) in $Mcu^{\Delta mye}$ and $Mcu^{fl/fl}$ imBMMs using a CRIPSR-Cas9–based genomic targeting strategy (18). CHMP4B deletion (Fig. 3 *C* and *D*) resulted in a complete abolishment of improved phagolysosomal integrity in silica-challenged $Mcu^{\Delta mye}$ imBMMs (Fig. 3*E*). Importantly, CHMP4B deletion also restored attenuated IL-1β production in $Mcu^{\Delta mye}$ imBMMs upon silica exposure without affecting IL-6 production (Fig. 3*F*). Deletion of CHMP3 in $Mcu^{\Delta mye}$ imBMMs (Fig. 3*G*) caused similar effects as CHMP4B deletion, including reversed phagolysosomal integrity (Fig. 3*H*) and restored IL-1β production (Fig. 3*I*) upon silica exposure. Taken together, these findings indicate that MCU promotes phagocytosis-triggered NLRP3 inflammasome activation by limiting ESCRT-dependent membrane repair of damaged phagolysosomes (*SI Appendix*, Fig. S4).

$Mcu^{\Delta mye}$ Mice Are Protected from Experimental Peritonitis. We next investigated the in vivo effect of MCU-mediated phagocytosis-triggered NLRP3 inflammasome activation by utilizing an alum-induced peritonitis model in our mice. Previous

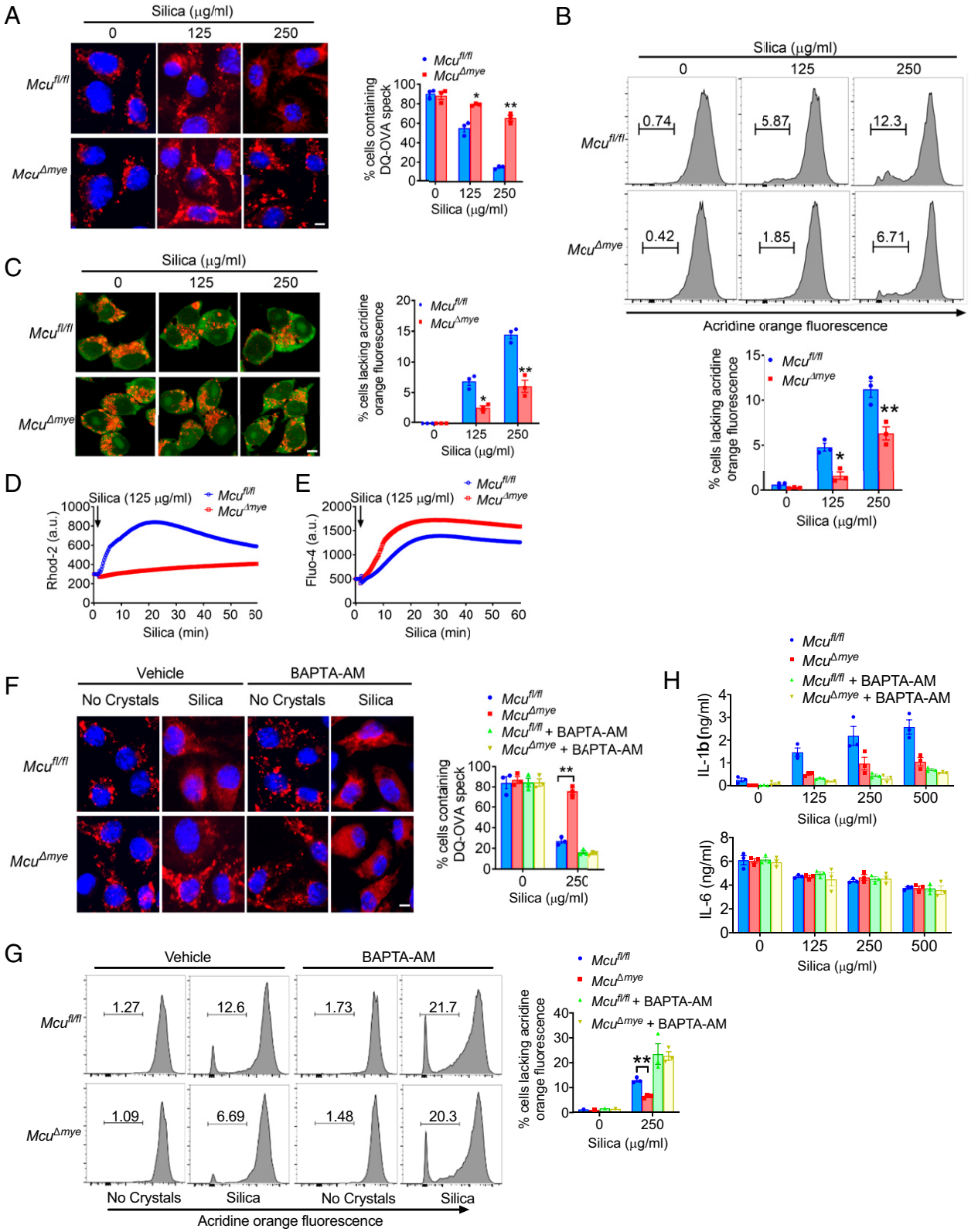

Fig. 2. MCU-dependent buffering of cytosolic Ca^{2+} promotes phagolysosomal leak. (*A*) Confocal imaging analysis (*Left*) and quantification (*Right*) of $Mcu^{fl/fl}$ or $Mcu^{\Delta mye}$ BMMs incubated with DQ ovalbumin (10 mg/mL) alone or together with silica. (*B*) Flow cytometry of $Mcu^{fl/fl}$ or $Mcu^{\Delta mye}$ BMMs stained with acridine orange and then treated with silica. Numbers (*Top*) and quantification (*Bottom*) indicate cells with lacking lysosomal staining of acridine orange. (*C*) Confocal imaging analysis (*Left*) and quantification (*Right*) of $Mcu^{fl/fl}$ or $Mcu^{\Delta mye}$ BMMs incubated with acridine orange and then treated with silica. (*D* and *E*) $Mcu^{fl/fl}$ or $Mcu^{\Delta mye}$ BMMs were incubated with Rhod-2 (*C*) or Fluo-4 (*D*) followed by silica stimulation. Fluorescence signal was read using a microplate reader. (*F*) Confocal imaging analysis (*Left*) and quantification (*Right*) of $Mcu^{fl/fl}$ or $Mcu^{\Delta mye}$ BMMs incubated with DQ ovalbumin, followed by treatment with BAPTA-AM (40 μM) for 15 min and then stimulated with silica. (*G*) Flow cytometry of $Mcu^{fl/fl}$ or $Mcu^{\Delta mye}$ BMMs stained with acridine orange and then treated with BAPTA-AM and silica. Numbers (*Left*) and quantification (*Right*) indicate cells lacking lysosomal staining of acridine orange. (*H*) $Mcu^{fl/fl}$ or $Mcu^{\Delta mye}$ BMMs were incubated with BAPTA-AM and then stimulated with silica for 4 h; IL-1β (*Top*) and IL-6 (*Bottom*) in supernatants were measured by ELISA. Values are expressed as mean ± SEM, and the results are representative of three independent experiments. (Scale bar, 2 μm.) Statistical analysis was determined by *t* test; $^*P < 0.05$, $^{**}P < 0.01$.

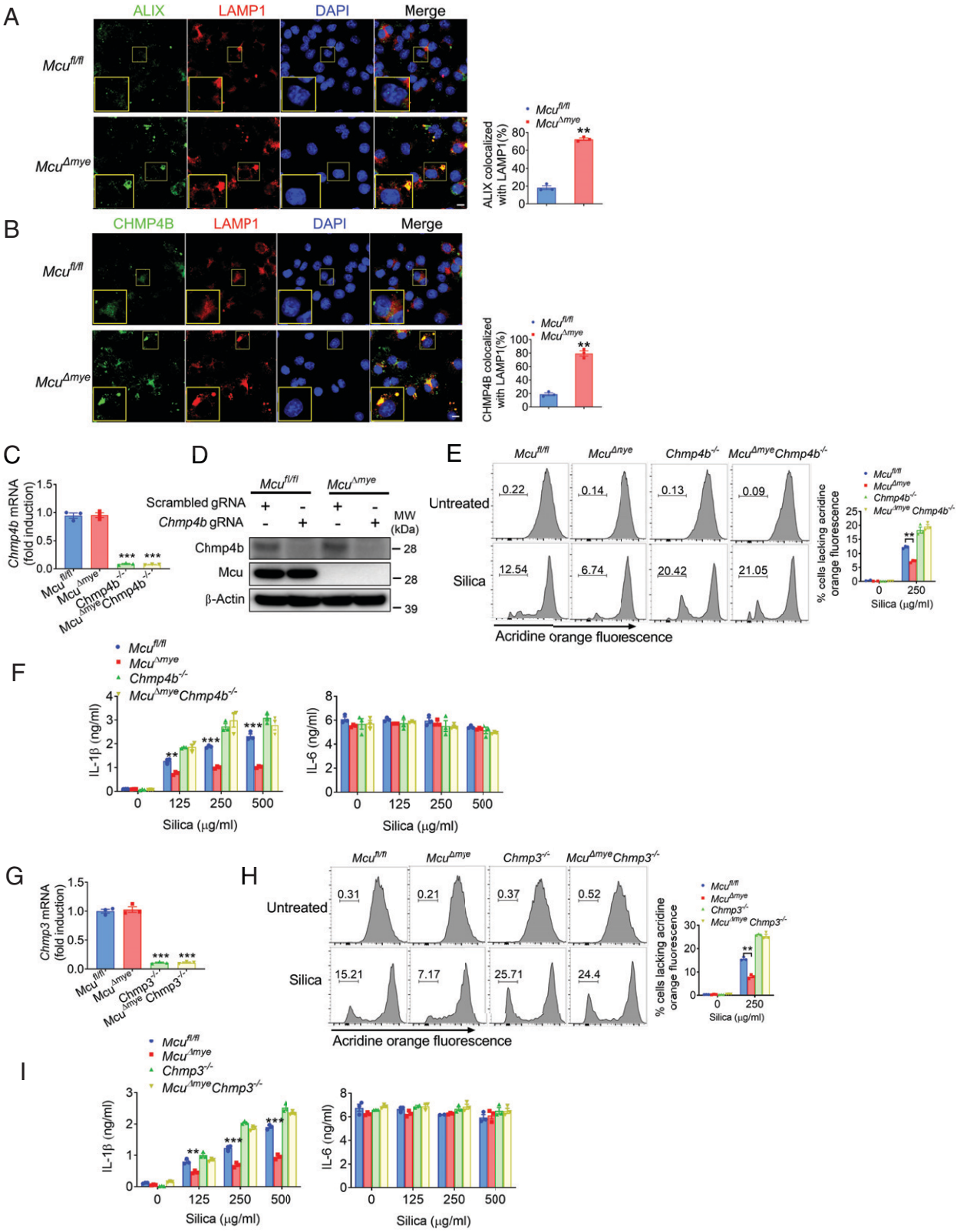

Fig. 3. The ESCRT complex attenuates phagocytosis-triggered NLRP3 inflammasome activation in $Mcu^{\Delta mye}$ macrophages. (*A* and *B*) Confocal imaging analysis (*Left*) and quantification (*Right*) of colocalization between ALIX or CHMP4B and phagosome. Cells were costained with anti-ALIX or anti-CHMP4B and anti-LAMP1 antibodies. Transcript (*C*) and protein level (*D*) of CHMP4B in CHMP4B knockout cells were measured by RT-PCR and immunoblotting, respectively. (*E*) Flow cytometry of $Mcu^{fl/fl}$, $Mcu^{\Delta mye}$, $Chmp4b^{-/-}$, or $Mcu^{\Delta mye}$ $Chmp4b^{-/-}$ BMMs stained with acridine orange and then treated with silica. Numbers (*Left*) and quantification (*Right*) indicate cells lacking lysosomal staining of acridine orange. (*F*) $Mcu^{fl/fl}$, $Mcu^{\Delta mye}$, $Chmp4b^{-/-}$, or $Mcu^{\Delta mye}$ $Chmp4b^{-/-}$ BMMs were stimulated with silica, and IL-1β and IL-6 production was measured by ELISA. Transcript (*G*) of CHMP3 in CHMP3 knockout cells was measured by RT-PCR. (*H*) Flow cytometry of $Mcu^{fl/fl}$, $Mcu^{\Delta mye}$, $Chmp3^{-/-}$, or $Mcu^{\Delta mye}$ $Chmp3^{-/-}$ BMMs stained with acridine orange and then treated with silica. Numbers (*Left*) and quantification (*Right*) indicate cells with lacking lysosomal staining of acridine orange. (*I*) $Mcu^{fl/fl}$, $Mcu^{\Delta mye}$, $Chmp3^{-/-}$, or $Mcu^{\Delta mye}$ $Chmp3^{-/-}$ BMMs were stimulated with silica; and IL-1β and IL-6 production was measured by ELISA. Values are expressed as mean ± SEM, and the results are representative of three independent experiments. (Scale bar, 2 μm.) Statistical analysis was determined by *t* test; $^{**}P < 0.01$, $^{***}P < 0.001$.

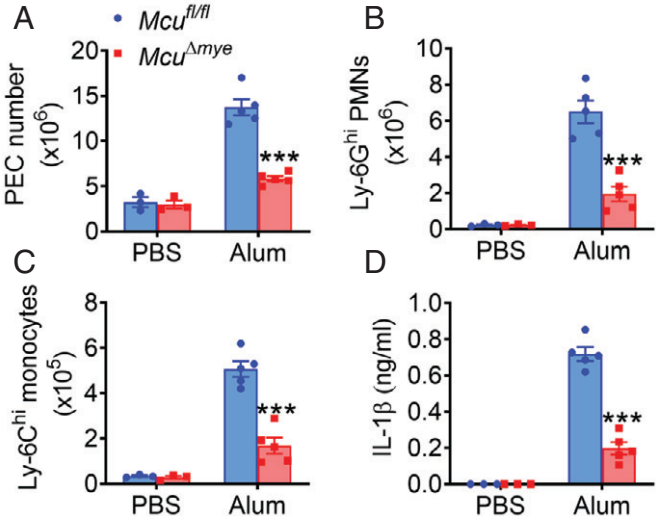

Fig. 4. *Mcu*$^{\Delta mye}$ mice are protected from alum-induced peritonitis. *Mcu*$^{fl/fl}$ and *Mcu*$^{\Delta mye}$ mice were intraperitoneally injected with alum (400 μg per mouse) diluted in sterile PBS. Peritoneal lavage was performed 16 h later. Absolute number of peritoneal exudate cells (PEC) (*A*), CD11b$^+$Ly-6G$^+$ neutrophils (*B*), and CD11b$^+$Ly-6C$^+$ cell inflammatory monocytes (*C*) were evaluated by flow cytometry analysis. (*D*) *Mcu*$^{fl/fl}$ and *Mcu*$^{\Delta mye}$ mice were intraperitoneally injected with alum (600 μg per mouse). Four hours after alum injection, peritoneal lavage was performed and IL-1β was measured by ELISA. Values are expressed as mean ± SEM, and the results are representative of three independent experiments. Statistical analysis was determined by *t* test; ***$P \leq 0.001$.

studies have documented that intraperitoneal injection of alum induces IL-1 signaling–dependent inflammatory cell recruitment (34, 35). As expected, we observed increased cell numbers (Fig. 4*A*) in peritoneal cavities of WT mice following a single intraperitoneal injection of alum, including Ly-6G$^+$ neutrophils (Fig. 4*B*) and Ly-6C$^+$ inflammatory monocytes (Fig. 4*C*). However, *Mcu*$^{\Delta mye}$ mice showed significantly less recruitment of immune cells, supporting a critical proinflammatory role of MCU in myeloid cell–mediated peritonitis. Furthermore, *Mcu*$^{\Delta mye}$ mice generated significantly less IL-1β in the peritoneal cavity 4 h after alum intraperitoneal injection (Fig. 4*D*). Overall, this study suggests that MCU in myeloid cells is important for inflammasome-mediated cytokine responses both in vitro and in vivo.

Discussion

In this study, we demonstrated that following phagocytosis of crystalline materials, deletion of MCU promotes Ca^{2+}-dependent recruitment of ESCRT proteins to damaged the phagolysosomal membrane and enhances membrane repair. This improved phagolysosome integrity results in attenuated activation of the downstream NLRP3 inflammasome in *Mcu*$^{\Delta mye}$ macrophages, consistent with previous studies showing an essential role of phagolysosome rupture promoting NLRP3 inflammasome activation (5, 36). Recent studies have revealed an intimate mitochondria–phagolysosome interaction during phagocytosis (37, 38). It has been suggested that mitochondria-derived signaling molecules such as metabolites and ions contribute to the functionality of phagolysosomes in a compartmentalized manner (17, 39). Phagolysosomes in macrophages contain much higher [Ca^{2+}] compared to the cytosolic compartment (40). When phagolysosomes are damaged due to the engulfment of undegradable particles, a rapid and transient Ca^{2+} flux from phagolysosomes to cytosol occurs, which is further buffered by MCU-mediated mitochondrial Ca^{2+} uptake (11). It has been well known that the elevation in $[Ca^{2+}]_{cyt}$ is required for ESCRT-dependent membrane repair (27, 31, 32). Therefore, it is expected that ESCRT-dependent phagolysosomal membrane repair is influenced by local Ca^{2+} levels in mitochondria–phagolysosome interaction sites. We indeed discovered that MCU-mediated cytosolic Ca^{2+} buffering antagonizes phagolysosomal recruitment of ESCRT proteins, exacerbates phagolysosomal rupture, and allows maximal activation of the downstream NLRP3 inflammasome. Importantly, we also found that phagocytosis-triggered activation of the NLRP3 inflammasome in the presence of MCU contributes to a proinflammatory effect in the alum-induced peritonitis model. Therefore, this study significantly expands our current understanding of the interaction between mitochondrial Ca^{2+} signaling and innate immune signaling.

In addition to the repair of leaky phagolysosomes, ESCRT machinery is also required for plasma membrane repair in a Ca^{2+}-dependent manner (26, 32). ESCRT-mediated plasma membrane repair counteracts activation of the NLRP3 inflammasome induced by ATP or nigericin, two phagocytosis-independent NLRP3 agonists (27). Our results suggest that MCU is uniquely required for phagocytosis-triggered, but not ATP- or nigericin-induced, activation of the NLRP3 inflamamsome, despite the fact that MCU-mediated mitochondrial Ca^{2+} uptake occurs in response to all of these stimuli (Fig. 2*D* and ref. 18). We reason that due to the close mitochondria–phagolysosomal interaction during phagocytosis, abolishment of MCU-mediated cytosolic Ca^{2+} buffering may enhance the formation of Ca^{2+} hot spots with high local [Ca^{2+}] around those interaction sites, which can efficiently stimulate the recruitment of the ESCRT complex to damaged phagolysosome for membrane repair. In contrast, upon plasma membrane damage, MCU-mediated cytosolic Ca^{2+} buffering is not able to efficiently counteract elevated local [Ca^{2+}] around damage sites due to minimal interactions between mitochondria and the plasma membrane. Indeed, our recent study detected comparable cytosolic [Ca^{2+}] between WT and MCU-deficient cells in response to agents causing plasma membrane damage (18). Therefore, spatial buffering of cytosolic Ca^{2+} by MCU upon phagolysosomal rupture provides a reasonable explanation of the unique role of MCU in phagocytosis-triggered activation of the NLRP3 inflammasome.

Mitochondria have recently emerged at the forefront of the host innate immune response in inflammatory diseases (41). One important mechanism of mitochondria contributing to innate immune activation is the release of mitochondria-derived danger-associated molecular patterns (DAMPs) such as mitochondrial DNA and cardiolipin, which have been reported to promote NLRP3 inflammasome activation (42–45). Mitochondrial Ca^{2+} overload has been considered as a common mechanism to trigger mitochondrial damage, followed by cytosolic release of sequestered DAMPs (46). For example, MCU-dependent mitochondrial Ca^{2+} overload has been implicated in promoting mitochondrial damage and cardiomyocyte cell death in an experimental ischemia–reperfusion injury model (47, 48). Furthermore, mitochondrial Ca^{2+} uptake also contributes to abnormal dynamics and depolarization of mitochondria upon the challenge with intracellular bacteria (49). Therefore, it is possible that besides ESCRT-mediated phagolysosomal membrane repair, the release of mitochondrial DAMPs following MCU-dependent mitochondrial damage may initiate an additional innate immune signaling cascade(s) other than inflammasome. Due to the diversity of stimuli that can cause dysregulated intracellular Ca^{2+} mobilization, understanding the function of

MCU-controlled intra- and extramitochondrial signaling will likely provide scientific insights into the pathogenesis of many inflammatory diseases.

Materials and Methods

Mice. C57BL/6 mice, lysozyme M-Cre mice, and *Cybb*$^{-/-}$ mice were obtained from The Jackson Laboratory. GFP-LC3 transgenic mice (50), *Mcu*$^{fl/fl}$ mice (18), and *Rubcn*$^{-/-}$ mice (51) have been previously described. *Mcu*$^{\Delta mye}$ mice were generated by crossing *Mcu*$^{fl/fl}$ mice with lysozyme M-Cre mice (18). *Mcu*$^{\Delta mye}$*Cybb*$^{-/-}$ and *Mcu*$^{\Delta mye}$*Rubcn*$^{-/-}$ double knockout (DKO) mice were further generated by crossing *Mcu*$^{\Delta mye}$ mice with *Cybb*$^{-/-}$ mice and *Rubcn*$^{-/-}$ mice, respectively. All mice were housed in specific pathogen-free facilities and all in vivo experiments were conducted in accordance with the National Institutes of Health Guide for the Care and Use of Laboratory Animals and the Institutional Animal Care and Use Committee. The study was approved by the Ethics Committee of The Ohio State University and all procedures were conducted in accordance with the experimental animal guidelines of The Ohio State University.

Reagents and Antibodies. Ultrapure LPS, flagellin, nigericin, CpG oligonucleotide, and poly(dA:dT) were purchased from InvivoGen. Silica (MIN-U-SIL 15) was obtained from US Silica. ATP was from Sigma-Aldrich. Pam3Cys was from EMC Microcollections. X-tremeGENE HP DNA transfection reagent was from Roche. Transfection reagent Profect P1 was from Targeting Systems. Acridine Orange (L13159) was from Alfa Aesar. TRIzol reagent (15596018), BAPTA-AM (B1205), and Alexa Fluor 594-labeled zymosan particles (Z23374) were from Thermo Fisher Scientific. Antibodies for immunoblotting include anti-CHMP4B (13683-1-AP) from Proteintech; anti-IKKα (05-536) from Millipore; anti-Mcu (14997), anti-phospho-IkBα (S32), anti-phospho-IKKα/β (S176/180), anti-phospho-p65(S536), anti-p65, anti-phospho-ERK1/2 (T202/Y204), anti-phospho-JNK (T183/Y185), and anti-phospho-p38 (T180/Y182) from Cell Signaling Technology; anti-β-actin (sc-1615) from Santa Cruz Biotechnology; anti-NLRP3 (Cryo-2), anti-Asc (AL177), and anti-caspase-1 (AG-20B-0042) from Adipogen; and anti-IL-1β (AF-401-NA) from R&D Systems. Antibodies for the flow cytometry assay include anti-CD45-PE Cy7 (103114), anti-CD11b-FITC (101206), anti-Ly-6G-PB (127612), and anti-Ly-6C-PE (128008) from BioLegend.

Cell Culture and Stimulation. BMMs were generated in the presence of L-929 conditional medium. Immortalized BMMs were generated with J2 retrovirus (carrying the v-myc and v-raf oncogenes), as previously described (5). Cells were cultured in Dulbecco's Modified Eagle Medium complemented with 10% fetal bovine serum, 1 mM sodium pyruvate, 1 mM nonessential amino acid, 100 IU/mL penicillin/streptomycin and 2 mM L-glutamine. After pretreatment with ultrapure LPS (200 ng/mL) for 3 h, cells were stimulated with silica at indicated concentrations for 4 to 16 h and transfected with poly(dA:dT) (1 μg/mL) or flagellin (1 μg/mL) for 4 h. Poly(dA:dT) was transfected with X-tremeGENE at a mass-to-volume ratio of 1:2. Flagellin was transfected with Profect P1 at a mass-to-volume ratio of 1:5. For ATP or nigericin, cells were primed with LPS, followed by ATP (2 mM) or nigericin (10 μM) stimulation for 40 min. BMMs were stimulated with LPS (200 ng/mL), Pam3Cys (1 mg/mL), and CpG (2 mg/mL) for various periods as indicated in the figure legends. Supernatant and cell lysate were collected for enzyme-linked immunosorbent assay (ELISA), LDH release assay, and Western blot analysis, respectively. Cells were collected for RT-PCR analysis.

RT-PCR Analysis. Total RNA was extracted from in vitro cultured BMMs using TRIzol. cDNA synthesis was performed with Moloney murine leukemia virus reverse transcriptase (Invitrogen) at 38 °C for 60 min. Real-time PCR was performed using SYBR Green PCR Master Mix (Applied Biosystems) in a StepOnePlus detection system (Applied Biosystems). The fold difference in mRNA expression between treatment groups was determined by a standard delta-delta Ct method. *β-Actin* was analyzed as an internal control. The primer sequences of individual genes are listed in *SI Appendix*, Table S1.

Immunoblotting. Electrophoresis of proteins was performed by using the NuPAGE system (Invitrogen) according to the manufacturer's protocol. Briefly, cultured BMMs were collected and lysed with radioimmunoprecipitation assay buffer. Proteins were separated on a NuPAGE gel and transferred onto nitrocellulose membranes (Bio-Rad). Appropriate primary antibodies and HRP-conjugated secondary antibodies were used and proteins were detected using the Enhanced Chemiluminescent (ECL) reagent (Thermo Scientific). Images were acquired with the ChemiDoc MP System (Bio-Rad). The quantification of expression of active protein versus inactive forms for caspase-1 and IL-1β was analyzed with ImageJ.

ELISA. Cytokines in supernatant from in vitro cultured cells or peritoneal lavage from animal experiments were quantified using the ELISA set for mouse IL-1β (R&D Systems), IL-6, and TNF-α (BD Biosciences) according to the manufacturer's protocol.

LDH-Release Assay. BMMs were seeded on 96-well plates. After treatment with indicated stimuli, supernatants were collected and LDH activity was determined with the Cytotoxicity Detection Kit (LDH) (11644793001, Roche). Cells left untreated or treated with 1% Triton X-100 were used as negative and positive controls, respectively.

Phagolysosome Integrity Assay. Two well-established strategies were utilized, as previously described (5). For confocal microscopy assay, LPS-primed macrophages were fed with DQ-OVA (D-12053, Thermo Fisher Scientific) together with silica. Phagolysosomal leak was indicated by a spread cytosolic pattern of fluorescent DQ-OVA, instead of a localized small vesicle pattern. To quantify the degree of phagolysosomal rupture, macrophages were stained with 1 μg/mL acridine orange for 15 min, a fluorescent dye that stains acidic lysosomes. Phagolysosomal leak was indicated by the loss of acridine orange fluorescence by flow cytometry assay using a BD FACSCanto flow cytometer or by a confocal fluorescence microscope (Olympus Fluoview FV3000).

Ca^{2+} Measurement. BMMs grown on 96-well clear-bottom black plates were incubated with 5 mM Fluo-4 AM (F10471; Thermo Fisher Scientific) (2 h) or 2 μM rhod-2/AM (R1244, Thermo Fisher Scientific) (1 h) in extracellular medium. Then the cells were treated with the indicated triggering stimulus. The fluorescence was read using a SpectraMax iD5 microplate reader at 494/516 nm for Fluo-4, or at 552/581 nm for Rhod-2.

Confocal Microscopy. BMMs (1×10^5) were seeded in eight-well chamber slides (Thermo Fisher Scientific). After the treatment with different stimuli, cells were fixed with 4% paraformaldehyde and then permeabilized with 0.5% Triton X-100 for 15 min, followed by blocking with 1% bovine serum albumin and 0.1% Triton X-100 in phosphate-buffered saline (PBS) at 37 °C for 1 h. The samples were incubated with anti-ASC antibody (AL177, Adipogen), anti-ALIX antibody (634501, Biolegend), anti-CHMP4B antibody (13683-1-AP, Proteintech), and anti-LAMP1 antibody (1D4B, Developmental Studies Hybridoma Bank) in the blocking buffer overnight at 4 °C, followed by the incubation with Alexa Fluor 647 goat anti-rabbit antibody (A-21244, Thermo Fisher Scientific), Alexa Fluor 488 goat anti-rabbit antibody (A-11008, Thermo Fisher Scientific), or Alexa Fluor 568 goat anti-rat antibody (A-11077, Thermo Fisher Scientific) for 2 h at room temperature. Nuclei were stained with DAPI (H-1200, Vector Laboratories). To evaluate LAP formation, BMMs, generated from GFP-LC3 transgenic mice, were incubated with zymosan at a ratio of 8:1 (particle/cell), then GFP-LC3 puncta were detected. Images were acquired using a laser scanning confocal fluorescence microscope with a 60× objective (Olympus Fluoview FV3000).

CRISPR-Cas9 Knockdown. Mouse *Chmp3*-targeted single gRNA sequence, 5′-GTGAAAGATGCAGCCAAGAA and *Chmp4b*-targeted single gRNA sequence, 5′-AAGCCGCTGGATGGCCTCCT, were cloned into the lentiCRISPR v2 backbone (Addgene #52961). Lentiviruses were packaged in 293T cells using the envelope-vector pMDL and VSV-G packaging vector. Transduction of *Mcu*$^{fl/fl}$ and *Mcu*$^{\Delta mye}$ imBMMs was performed in the presence of polybrene. Single cell colonies were selected by unlimited dilution. Cells with effective *Chmp3* and *Chmp4b* deletion were used for further assays.

Plasmid and Molecular Cloning. To generate the lentivector expressing *MCU*, the vector pDONR223-*MCU* was obtained from the human ORFeome (http://horfdb.dfci.harvard.edu/) (accession no. BC034235). Full-length *MCU* was subcloned into the pWPXLd lentivector (Addgene #12258). The primers were listed as follows: forward 5′-AGCTTTGTTTAAACATGGCGGCCGCCGCAGGTA-3′ and reverse 5′-CGGGATCCCGATCTTTTTCACCAATTTGTC-3′. To reconstitute *Mcu*$^{\Delta mye}$ BMMs with *MCU*, cells were transduced with the lentivector encoding *MCU*.

Alum-Induced Peritonitis. *Mcu*$^{fl/fl}$ and *Mcu*$^{\Delta mye}$ mice were injected intraperitoneally with 400 μg of alum diluted in sterile PBS. Peritoneal lavage was performed 16 h later. The peritoneal exudate cells were stained with cell surface markers to count the neutrophil and inflammatory monocyte populations. The CD11b^{+}Ly-6G^{+} and CD11b^{+}Ly-6C^{+} cells were identified as neutrophils and monocytes, respectively. Flow cytometry analysis was performed by a BD FACSCanto flow cytometer. Alternatively, mice were injected with 600 μg of alum. Four hours after alum injection, peritoneal lavage was performed and IL-1β was measured by ELISA.

Statistical Analysis. Statistical analysis was carried out with Prism 8 for Macintosh. Results were presented as the mean ± SEM, and unpaired Student's *t* test (one tailed) was applied to evaluate significance. Comparisons between multiple time points were analyzed by repeated-measurements analysis of variance with Bonferroni posttests. *P* values less than 0.05 were considered statistically significant.

Data Availability. All study data are included in the article and/or *SI Appendix*.

ACKNOWLEDGMENTS. We thank Dr. Douglas Green (St. Jude Children's Research Hospital) for providing GFP-LC3 transgenic mice and *Rubcn*$^{-/-}$ mice, Dr. Katherine Fitzgerald (University of Massachusetts) for J2 retrovirus. This work was supported by NIH Grants R01GM120496 and R01GM135234 (H.W.).

1. B. K. Davis, H. Wen, J. P. Ting, The inflammasome NLRs in immunity, inflammation, and associated diseases. *Annu. Rev. Immunol.* **29**, 707–735 (2011).
2. S. M. Man, T. D. Kanneganti, Converging roles of caspases in inflammasome activation, cell death and innate immunity. *Nat. Rev. Immunol.* **16**, 7–21 (2016).
3. P. Broz, V. M. Dixit, Inflammasomes: Mechanism of assembly, regulation and signalling. *Nat. Rev. Immunol.* **16**, 407–420 (2016).
4. P. Orning, E. Lien, K. A. Fitzgerald, Gasdermins and their role in immunity and inflammation. *J. Exp. Med.* **216**, 2453–2465 (2019).
5. V. Hornung *et al.*, Silica crystals and aluminum salts activate the NALP3 inflammasome through phagosomal destabilization. *Nat. Immunol.* **9**, 847–856 (2008).
6. S. C. Eisenbarth, O. R. Colegio, W. O'Connor, F. S. Sutterwala, R. A. Flavell, Crucial role for the Nalp3 inflammasome in the immunostimulatory properties of aluminium adjuvants. *Nature* **453**, 1122–1126 (2008).
7. R. Muñoz-Planillo *et al.*, K^{+} efflux is the common trigger of NLRP3 inflammasome activation by bacterial toxins and particulate matter. *Immunity* **38**, 1142–1153 (2013).
8. G. S. Lee *et al.*, The calcium-sensing receptor regulates the NLRP3 inflammasome through Ca2+ and cAMP. *Nature* **492**, 123–127 (2012).
9. Z. Zhong *et al.*, TRPM2 links oxidative stress to NLRP3 inflammasome activation. *Nat. Commun.* **4**, 1611 (2013).
10. M. Rossol *et al.*, Extracellular Ca2+ is a danger signal activating the NLRP3 inflammasome through G protein-coupled calcium sensing receptors. *Nat. Commun.* **3**, 1329 (2012).
11. T. Murakami *et al.*, Critical role for calcium mobilization in activation of the NLRP3 inflammasome. *Proc. Natl. Acad. Sci. U.S.A.* **109**, 11282–11287 (2012).
12. J. G. McCormack, A. P. Halestrap, R. M. Denton, Role of calcium ions in regulation of mammalian intramitochondrial metabolism. *Physiol. Rev.* **70**, 391–425 (1990).
13. D. De Stefani, A. Raffaello, E. Teardo, I. Szabò, R. Rizzuto, A forty-kilodalton protein of the inner membrane is the mitochondrial calcium uniporter. *Nature* **476**, 336–340 (2011).
14. J. M. Baughman *et al.*, Integrative genomics identifies MCU as an essential component of the mitochondrial calcium uniporter. *Nature* **476**, 341–345 (2011).
15. R. Rizzuto, D. De Stefani, A. Raffaello, C. Mammucari, Mitochondria as sensors and regulators of calcium signalling. *Nat. Rev. Mol. Cell Biol.* **13**, 566–578 (2012).
16. D. De Stefani, R. Rizzuto, T. Pozzan, Enjoy the trip: Calcium in mitochondria back and forth. *Annu. Rev. Biochem.* **85**, 161–192 (2016).
17. I. Drago, D. De Stefani, R. Rizzuto, T. Pozzan, Mitochondrial Ca2+ uptake contributes to buffering cytoplasmic Ca2+ peaks in cardiomyocytes. *Proc. Natl. Acad. Sci. U.S.A.* **109**, 12986–12991 (2012).
18. T. Li *et al.*, Listeria monocytogenes upregulates mitochondrial calcium signalling to inhibit LC3-associated phagocytosis as a survival strategy. *Nat. Microbiol.* **6**, 366–379 (2021).
19. A. Rimessi *et al.*, Mitochondrial Ca2+-dependent NLRP3 activation exacerbates the Pseudomonas aeruginosa-driven inflammatory response in cystic fibrosis. *Nat. Commun.* **6**, 6201 (2015).
20. A. Rimessi *et al.*, Pharmacological modulation of mitochondrial calcium uniporter controls lung inflammation in cystic fibrosis. *Sci. Adv.* **6**, eaax9093 (2020).
21. K. Triantafilou, S. Kar, F. J. van Kuppeveld, M. Triantafilou, Rhinovirus-induced calcium flux triggers NLRP3 and NLRC5 activation in bronchial cells. *Am. J. Respir Cell Mol. Biol.* **49**, 923–934 (2013).
22. M. L. Skowyra, P. H. Schlesinger, T. V. Naismith, P. I. Hanson, Triggered recruitment of ESCRT machinery promotes endolysosomal repair. *Science* **360**, eaar5078 (2018).
23. M. Radulovic *et al.*, ESCRT-mediated lysosome repair precedes lysophagy and promotes cell survival. *EMBO J.* **37**, e99753 (2018).
24. C. Raiborg, H. Stenmark, The ESCRT machinery in endosomal sorting of ubiquitylated membrane proteins. *Nature* **458**, 445–452 (2009).
25. J. Schöneberg, I. H. Lee, J. H. Iwasa, J. H. Hurley, Reverse-topology membrane scission by the ESCRT proteins. *Nat. Rev. Mol. Cell Biol.* **18**, 5–17 (2017).
26. A. J. Jimenez *et al.*, ESCRT machinery is required for plasma membrane repair. *Science* **343**, 1247136 (2014).
27. S. Rühl *et al.*, ESCRT-dependent membrane repair negatively regulates pyroptosis downstream of GSDMD activation. *Science* **362**, 956–960 (2018).
28. Y. N. Gong *et al.*, ESCRT-III acts downstream of MLKL to regulate necroptotic cell death and its consequences. *Cell* **169**, 286–300.e16 (2017).
29. M. A. Sanjuan *et al.*, Toll-like receptor signalling in macrophages links the autophagy pathway to phagocytosis. *Nature* **450**, 1253–1257 (2007).
30. M. A. Katsnelson, L. G. Rucker, H. M. Russo, G. R. Dubyak, K+ efflux agonists induce NLRP3 inflammasome activation independently of Ca2+ signaling. *J. Immunol.* **194**, 3937–3952 (2015).
31. N. W. Andrews, P. E. Almeida, M. Corrotte, Damage control: Cellular mechanisms of plasma membrane repair. *Trends Cell Biol.* **24**, 734–742 (2014).
32. L. L. Scheffer *et al.*, Mechanism of Ca^{2+}-triggered ESCRT assembly and regulation of cell membrane repair. *Nat. Commun.* **5**, 5646 (2014).
33. T. Li *et al.*, O-GlcNAc transferase links glucose metabolism to MAVS-mediated antiviral innate immunity. *Cell Host Microbe* **24**, 791–803.e6 (2018).
34. G. Guarda *et al.*, Type I interferon inhibits interleukin-1 production and inflammasome activation. *Immunity* **34**, 213–223 (2011).
35. C. Zhao, D. D. Gillette, X. Li, Z. Zhang, H. Wen, Nuclear factor E2-related factor-2 (Nrf2) is required for NLRP3 and AIM2 inflammasome activation. *J. Biol. Chem.* **289**, 17020–17029 (2014).
36. A. Halle *et al.*, The NALP3 inflammasome is involved in the innate immune response to amyloid-beta. *Nat. Immunol.* **9**, 857–865 (2008).
37. B. H. Abuaita, T. L. Schultz, M. X. O'Riordan, Mitochondria-derived vesicles deliver antimicrobial reactive oxygen species to control phagosome-localized Staphylococcus aureus. *Cell Host Microbe* **24**, 625–636.e5 (2018).
38. A. P. West *et al.*, TLR signalling augments macrophage bactericidal activity through mitochondrial ROS. *Nature* **472**, 476–480 (2011).
39. W. Peng, Y. C. Wong, D. Krainc, Mitochondria-lysosome contacts regulate mitochondrial Ca^{2+} dynamics via lysosomal TRPML1. *Proc. Natl. Acad. Sci. U.S.A.* **117**, 19266–19275 (2020).
40. K. A. Christensen, J. T. Myers, J. A. Swanson, pH-dependent regulation of lysosomal calcium in macrophages. *J. Cell Sci.* **115**, 599–607 (2002).
41. A. P. West, G. S. Shadel, S. Ghosh, Mitochondria in innate immune responses. *Nat. Rev. Immunol.* **11**, 389–402 (2011).
42. K. Nakahira *et al.*, Autophagy proteins regulate innate immune responses by inhibiting the release of mitochondrial DNA mediated by the NALP3 inflammasome. *Nat. Immunol.* **12**, 222–230 (2011).
43. A. P. West, G. S. Shadel, Mitochondrial DNA in innate immune responses and inflammatory pathology. *Nat. Rev. Immunol.* **17**, 363–375 (2017).
44. K. Shimada *et al.*, Oxidized mitochondrial DNA activates the NLRP3 inflammasome during apoptosis. *Immunity* **36**, 401–414 (2012).
45. S. S. Iyer *et al.*, Mitochondrial cardiolipin is required for Nlrp3 inflammasome activation. *Immunity* **39**, 311–323 (2013).
46. C. Giorgi, S. Marchi, P. Pinton, The machineries, regulation and cellular functions of mitochondrial calcium. *Nat. Rev. Mol. Cell Biol.* **19**, 713–730 (2018).
47. J. Q. Kwong *et al.*, The mitochondrial calcium uniporter selectively matches metabolic output to acute contractile stress in the heart. *Cell Rep.* **12**, 15–22 (2015).
48. T. S. Luongo *et al.*, The mitochondrial calcium uniporter matches energetic supply with cardiac workload during stress and modulates permeability transition. *Cell Rep.* **12**, 23–34 (2015).
49. F. Stavru, F. Bouillaud, A. Sartori, D. Ricquier, P. Cossart, Listeria monocytogenes transiently alters mitochondrial dynamics during infection. *Proc. Natl. Acad. Sci. U.S.A.* **108**, 3612–3617 (2011).
50. N. Mizushima, Methods for monitoring autophagy using GFP-LC3 transgenic mice. *Methods Enzymol.* **452**, 13–23 (2009).
51. J. Martinez *et al.*, Molecular characterization of LC3-associated phagocytosis reveals distinct roles for Rubicon, NOX2 and autophagy proteins. *Nat. Cell Biol.* **17**, 893–906 (2015).